# H2-selective Troger's base-based Mixed Matrix Membranes Enhanced by 2D MOFs

Jing Deng†, Zhongde Dai† and Liyuan Deng*

Department of Chemical Engineering, Norwegian University of Science and Technology, 7491 Trondheim, Norway

E-mail: deng@nt.ntnu.no,  Tel.: +47 73594112

† These authors contributed equally.

## Abstract

In this work, two two-dimensional (2D) leaf-like ZIFs (ZIF-L-Zn and ZIF-L-Co) were incorporated into the Troger's base (TB)-based polymers for hydrogen separation. SEM imaging and enhanced performance have demonstrated good dispersion of leaf ZIFs in the resultant mixed matrix membranes (MMMs), thanks to the good compatibility between polymeric matrix and nanoleaves. The addition of both leaf ZIFs greatly enhances the gas permeabilities of all investigated species within the studied loading. Thanks to the interlayer channels in the laminated 2D ZIFs, small molecules like $H_2$ obtain additional fast transport pathway and, thus, a remarkable increase in gas permeability up to 4 times. A $H_2$ permeability of 1235.5 Barrer was achieved in the presence of 20 wt.% ZIF-L-Co. Compared with ZIF-L-Zn, ZIF-L-Co is more efficient in promoting gas permeabilites with similar selectivities for all gas pairs. The MMMs with ZIF-L-Co have displayed excellent hydrogen separation performances, which surpass all Upper Bounds of $H_2/CO_2$, $H_2/N_2$ and $H_2/CH_4$. Further increasing the operating temperature enhances the gas transport properties, and the membrane with 20 wt.% ZIF-L-Co at 60 °C gives a $H_2$ permeability up to 1985.9 Barrer, which is 6.8 times greater than that of the neat polymer membrane at room temperature.

## Keywords:

Leaf ZIFs; Troger's base polymer; mixed matrix membranes; hydrogen separation

# 1 Introduction

Hydrogen ($H_2$), recognized as one of the cleanest energy sources, has been utilized as an energy source in fuel cells or the starting materials for the syntheses of various chemicals [1-3]. The demands for clean and sustainable energy have grown exponentially, and the hydrogen market, which was valued at around $108.1 billion in 2016, has been estimated to reach $180.2 billion by 2025 [4]. Despite its abundance on earth, $H_2$ cannot be obtained naturally, and the major production technique currently is the steam methane reforming based on fossil fuel or natural gas [5-7]. The synthesized $H_2$ needs to be purified from the $H_2/CO_2$ mixture before being used in various industrial applications (e.g., methanol or ammonia production). Generally speaking, in these applications, the reactant $H_2$ needs to be separated from the product mixture and re-cycled to ensure a high process efficiency and a high product yield. Therefore, $H_2$ separation from various gas mixture is extremely crucial. Considering the huge market size, any improvement in $H_2$ purification will bring significant benefits.

The gas membrane technology has a much lower energy consumption rate, smaller footprints and simpler operation than the major conventional separation method (i.e., liquid absorption). However, current $H_2$-selective polymeric membranes are limited to a few materials, since most polymeric materials usually have very low $H_2$ permeabilities (< 100 Barrer) or $H_2$ selectivities ($H_2/N_2$ selectivity of ~ 2 for PTMSP and ~ 10 for PIM-1; $H_2/CH_4$ selectivity of ~ 1 for PTMSP and ~ 10 for PIM-1) [8, 9]. According to the solution-diffusion theory, materials with high free volume and narrow porous element distribution may achieve high $H_2$ permeability and high $H_2$ selectivity at the same time. Therefore, recently developed materials with more free volume elements have been intensively employed to realize higher gas diffusion and, thus, higher gas permeability without sacrificing high selectivity. Based on the polymer structure, decreasing chain mobility by introducing bulky and contorted units could generate more free volume and thus lead to better separation performance [10]. This is mostly seen in polymers with intrinsic microporosity (PIM). Since the excellent separation performance of PIMs was first reported [11], many contorted and inflexible units have been developed and incorporated into polymer structure for membrane separation purposes [12]. In 2013, Mckeown and coworkers found that PIMs containing bridged bicyclic amine, usually called Troger's base (TB), could have particularly high gas permeability and considerably high gas selectivity, which exceed or are close to the Upper Bounds for several gas pairs [13]. Further analysis was carried out and the results show that the dihedral angle at the

center of the TB ($120^\circ$) is much higher than that at the center of the spirobisindane ($\sim 90^\circ$), usually known as units of PIM-1, thus resulting in more rigid chains, less efficient packing and higher gas permeability. It is worth noting that the synthesis of TB units is relatively easy and simple, and the resultant polymers are usually soluble in many organic solvents. Recent studies have enlarged the family of TB-based polymers to include polyimide copolymer [14-18], or polymers containing only TB units [19, 20]. These TB-based polymers generally have high gas permeability for small molecules because of the contorted chains. In addition, due to their narrow distribution of free volume elements, their selectivities for various gas pairs (e.g.: $H_2/N_2$: $\sim 50$) are rather high compared to other polymers with high gas permeabilities.

Recently, introducing inorganic materials into polymeric matrix has aroused plenty of attention as it combines the excellent $H_2$ separation performance of the inorganic materials and the good processability of polymeric matrix [21-24]. Some studies have reported this method's effectiveness in promoting the $H_2$ separation performance. Song *et al.* reported that by mixing two different nanoparticles (nonporous $SiO_2$ and microporous ZIF-8) with PIM-1, $H_2$ permeability was enhanced from around 3361 Barrer to 5456 Barrer with a slight increase in $H_2/N_2$ and $H_2/CH_4$ selectivities [22]. The large increment in $H_2$ permeability is mainly as a result of the increased diffusion, which could be explained by several factors. First, the incorporation of nanofillers disrupts the packing arrangement of rigid polymer and, thus, changes the porous elements in the membranes. The interfaces between the inorganic particles and the polymeric matrix also enhance the gas diffusion. Moreover, the well-designed structure of these inorganic fillers may contribute extra transport channels for $H_2$ transport. The authors compared two different nanoparticles and found that the porous ZIF-8s could offer extra transport channels for small molecules like $H_2$, thus obtaining higher $H_2$ permeabilities, compared with the nonporous silica. The overall performances surpass the Upper Bounds for several gas pairs, like $H_2/N_2$ and $H_2/CH_4$. Some well-designed nanoparticles also have been reported could provide great benefits for this application. Wang and coworkers incorporated the ZIF-Ls into a polyimide (PI) matrix for gas separation [23]. The gas permeation results show this combination offers a greatly increased $H_2$ permeability and selectivity, and these enhancements are mainly caused by the aligned interlayer channels in the 2D ZIF-L with a size of 3.1 Å, which could block the bigger molecules (i.e., $CO_2$), but not the smaller ones (i.e., $H_2$) that can pass freely.

Hence, in this work, the heterocyclic TB-based polymer was chosen as the polymeric matrix. Two leaf-like ZIFs (ZIF-L-Zn and ZIF-L-Co) were incorporated into the TB-based polymer to prepare a series of TB + leaf-like ZIFs MMMs. The influence of these leaf-like ZIFs on the material properties and the $H_2$ separation performance of the resultant MMMs were studied. Various methods, like thermal gravimetric analysis (TGA), Fourier-transform infrared spectroscopy (FTIR), scanning electron microscope (SEM) and single gas permeation experiments, were employed. The gas transport properties, with respect to $H_2$, $CO_2$, $N_2$, and $CH_4$, of the resultant MMMs were systematically assessed, and the ideal selectivity for various gas pairs were also studied. Moreover, the effects of permeation operating temperature were studied.

## 2 Experimental section

### 2.1. Materials

$Zn(NO_3)_2 \cdot 6H_2O$, $Co(NO_3)_2 \cdot 6H_2O$ and 2-methylimidazole (Hmim) were ordered from Sigma, Norway. Tolidine, dimethoxymethane (DMM), trifluoroacetic acid (TA), ammonium hydroxide solution (28%) and methylpyrrolidone (NMP) were also purchased from Sigma, Norway. Methanol was bought from VWR, Norway. All the chemicals were used without further treatment.

### 2.2. Leaf ZIFs and TB polymer synthesis

The preparation of ZIF-L-Zn followed the method developed by Wang et al. [25]. Typically, 0.59 g of $Zn(NO_3)_2 \cdot 6H_2O$ and 1.30 g of Hmim were dissolved in 40 mL deionized (DI) water respectively, and then the two solutions were mixed and stirred for 3 h at room temperature. For the preparation of ZIF-L-Co, 0.7275g of $Co(NO_3)_2 \cdot 6H_2O$ was dissolved in 50 mL DI water for 10 min, and 2.4025g of Hmim was dissolved in another 50 ml DI water for 10 min. Afterwards, the two solutions were mixed and stirred for 30 min. White ZIF-L-Zn and purple ZIF-L-Co leaf were obtained by filtering the respective mixtures using a vacuum filtration assembly (VWR) equipped with a PVDF filter membrane (pore size of 0.65 μm). The obtained ZIFs were dried in vacuum oven for 12 hours at 60 °C.

The TB polymer was synthesized, according to a procedure reported previously by Li et al. [19, 20], as shown in **Scheme 1**. Under a $N_2$ atmosphere, 20 g o-Tolidine and 36 g DMM were mixed in a 500 mL three-necked flask, which was placed in an ice-water bath. Afterwards, 200 mL of trifluoroacetic acid (TFA) was added in drops into the mixture within 30 min. Thereafter, the mixture was stirred at ambient conditions for 48 h. Then the polymerization was stopped by slowly

4

pouring the solution into 2L aqueous ammonium hydroxide solution (5 wt. %). The precipitated polymer was washed with excess DI water until the pH was close to 7, and then dried in a vacuum oven for 12 hours at 80 °C. The polymer was further purified by dissolving in NMP (~10 wt.%) and re-precipitating twice in methanol. Finally, the polymer was dried again in a vacuum oven for 12 hours at 80 °C.
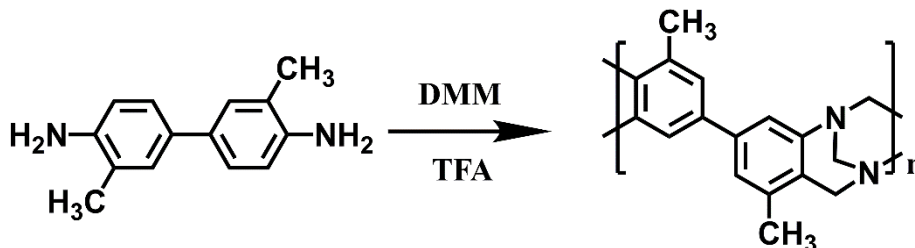


**Scheme 1** The synthesis of TB polymer.

## 2.3. MMMs fabrication

MMMs were prepared through a knife casting method. Typically, the desired amount of dried leaf-like ZIFs were added into 5 ml NMP and stirred overnight until a well-dispersed suspension was obtained. Then the desired amount of TB polymer was added into the ZIF suspension and the total solid (i.e., TB + ZIFs) concentration was around 10 wt. %. Thereafter, the membrane solution was cast on a glass plate using a casting knife (PA-4302, BYK-CHEMIE GMBH, Germany), with a wet gap of ~ 600 µm. The cast membrane was then heated to 80 °C in vacuum for 24 h to evaporate NMP. To completely remove the solvent, the resulting membranes were immersed in methanol for 12 h at room temperature. Finally, the membranes were dried overnight in a vacuum oven at 60 °C.

## 2.4. Characterization

The morphology of the leaf ZIFs and MMMs was studied using a SEM (TM3030 tabletop microscope, Hitachi High Technologies). Surface samples of MMMs were prepared using scissors and cross-section specimens were prepared by breaking the samples in liquid $N_2$. All the samples were sputter-coated with gold for 2 minutes before SEM experiments to ensure good electrical conductivity.

The thermal stability of the leaf ZIFs and the resultant MMMs was evaluated by TGA (TG 209F1 Libra, Netzsch). Samples with 10 ~ 20 mg were tested from room temperature to 800 °C in $N_2$ atmosphere.

XRD (D8 A25 DaVinci, Bruker) was employed for the analysis of the crystallinity of the leaf ZIFs, as well as that of the resultant MMMs. The source was offered by Cu (Kα radiation) and the characteristic wavelength λ is 1.54 Å. The scans were taken in the 2θ range from 5° to 75°.

FTIR spectroscopy was carried out using a Thermo Nicolet Nexus spectrometer with a smart endurance reflection cell. The spectra averaged over 16 scans at a wavenumber resolution of 4 cm$^{-1}$ from 550 cm$^{-1}$ to 4000 cm$^{-1}$.

Single gas permeation tests were performed by the constant-volume variable-pressure method, with a feed pressure of around 2 bar at various temperatures. For the operating temperatures higher than room temperature (24 °C), a temperature control system is equipped in the single gas permeation setup to maintain the desired temperatures. The gas permeabilities ($P$) were calculated as shown in equation (1):

$$P = \left[\left(\frac{dp_d}{dt}\right)_{t\to\infty} - \left(\frac{dp_d}{dt}\right)_{leak}\right] \cdot \frac{V_d}{A \cdot R \cdot T} \cdot \frac{l}{(p_u - p_d)} \tag{1}$$

where $P$ is the permeability (in Barrer), $p_d$ and $p_u$ are the downstream (~2 bar) and upstream pressure (0 – 100 mbar), respectively, $t$ refers to time, $V_d$ is the downstream volume, $A$ means the effective permeation area of membrane, $R$ and $T$ are the ideal gas constant and temperature, respectively, and $l$ is the thickness of membrane. The leakage rate ($dp_d/dt$)$_{leak}$ is the downstream pressure increasing rate, which is measured at the permeate side after being vacuumed for a certain period of time. The feed side is isolated in membrane cell using alumina foil from the permeate side and filled with N$_2$ at 2 bar. The leakage rate is at least two orders of magnitude lower than the pressure increasing rate caused by the gas permeation ($d_p/d_t$) in the current work. The thicknesses of all membranes were measured by an ABS Digimatic Indicator (Mitutoyo, Suzhou, China). They were given by the average of more than 10 measurements for each membrane. The typical thicknesses of the obtained membranes are 50 ± 10 µm. To maintain nearly constant driving force (p$_u$-p$_d$), the downstream pressure was limited within 100 mbar by employing suitable downstream volume, and the upstream pressure was almost constant during permeation test because of the large capacity of the upstream gas tank. The permeability was the average values obtained from at least 2 samples with a relative error of less than 10%.

The ideal selectivity of gas A over gas B ($\alpha_{A/B}$) was calculated using equation 2:

$$\alpha_{A/B} = \frac{P_A}{P_B} \tag{2}$$

6

Furthermore, the diffusivity (*D*) was calculated according to the time-lag method (equation 3), and the time-lag (*θ*) is obtained from each single permeation test:

$$D = \frac{l^2}{6 \cdot \theta}$$

(3)

Based on the solution-diffusion mechanism, the solubility (*S*) was calculated from the permeability and the diffusivity values:

$$S = \frac{P}{D}$$

(4)

# 3 Results and discussion

## 3.1. Characterization of Leaf ZIFs

The SEM images of the morphology of the two as-prepared leaf ZIFs are shown in **Figure 1 (A)-(B)**. These ZIF-L-Zn and ZIF-L-Co display a leaf-like shape with a size of $1.3 \times 5.4$ µm and $1.6 \times 5.6$ µm, respectively, similar with a previous report [25]. A BET surface area of 162.9 $m^2$/g and 12.5 $m^2$/g was obtained for ZIF-L-Zn and ZIF-L-Co, respectively, from $N_2$ adsorption experiments, and these results are comparable to the values reported in the previous literature (BET surface area lower than 200 $m^2$/g for ZIF-L-Zn [25-27] and 20 $m^2$/g for ZIF-L-Co [28]). Interestingly, both adsorbed $N_2$ amount (**Figure 1(C)**), and the surface area of ZIF-L-Co are lower than that of ZIF-L-Zn. Regarding the identical structure and arrangement of the crystal units, the possible reason may be the narrower interlayer channels of ZIF-L-Co. To further confirm the structure of these as-prepared ZIFs, XRD analysis was employed. As shown in **Figure 1(D)**, the obtained XRD curves of both ZIFs are very similar to the reported experimental or simulated pattern by Wang and co-workers. [25]. Because of the same crystal construction, the crystal units of both leaf ZIFs are theoretically the same, which result in almost identical XRD patterns. The chemical nature of the ZIFs is evaluated by FTIR spectroscopy, and the resultant spectra are displayed in **Figure S1.** The main characteristic peaks of these ZIFs are associated with the Hmim units: the peaks at 1567 $cm^{-1}$, 1305 $cm^{-1}$ and 995 $cm^{-1}$ refer to the C=N bonds and C-N bond, respectively, and the broad ones at 3500 – 2500 $cm^{-1}$ suggest the N–H···N hydrogen bonds between Hmim units. Since these ZIFs have the same organic ligand, their spectra are almost identical despite the different metal ions.

That is because that the absorbance peak of metal ions – Hmim is reported to be around 400 cm$^{-1}$ [29], which exceeds the tested range of the used FTIR.
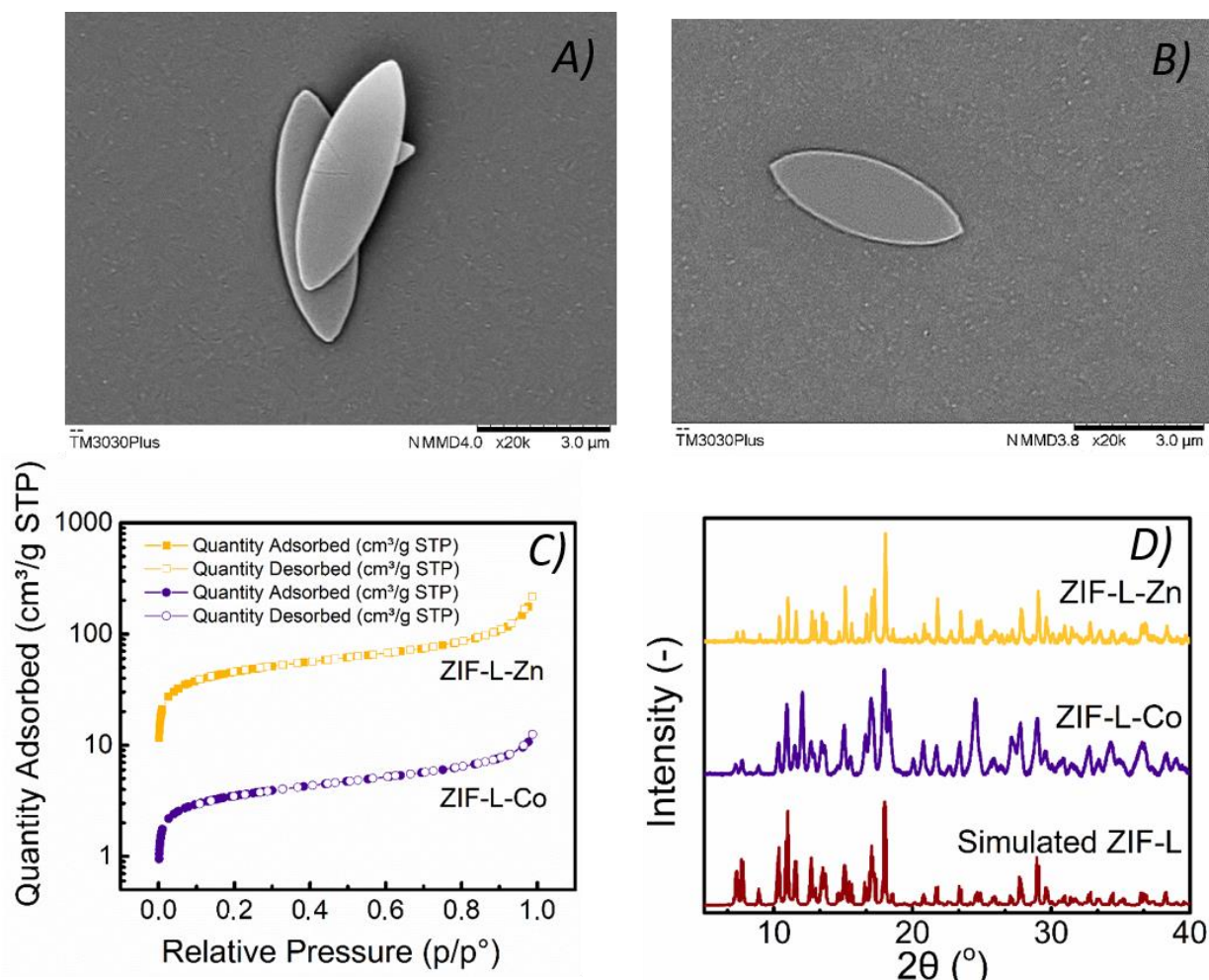


**Figure 1** SEM image of A) ZIF-L-Zn and B) ZIF-L-Co, and the C) N$_2$ adsorption, and D) XRD results of ZIF-L-Zn and ZIF-L-Co.

The thermal decomposition behaviors of both ZIFs are quite similar, as shown in **Figure S2**. A small weight loss (< 3 %) is observed at temperature below 100 °C because of the remaining solvent, followed by loss of structural water molecules and Hmim in the ZIFs [26, 27], which explains the sharp decrease at temperature around 230 - 250 °C. Then there is a collapse in the crystal structure of the ZIFs when the temperature reaches 500 °C, presented by the second sharp slope. Generally speaking, the ZIF-L-Co starts losing structural units slightly earlier than the ZIF-L-Zn. Considering that most applications of membrane gas separation have an operating

temperature of 60 °C or even lower, both ZIFs could fulfill the temperature requirements as membrane materials.

## 3.2. Characterization of the MMMs

### 3.2.1. Physical and chemical property characterization

*FTIR*

FTIR analysis was employed to study the chemical nature of the as-synthesized polymer and the resultant MMMs, and the results are presented in **Figure 2**. For the neat TB polymer, the absorbance bands at 2900 – 3000 cm$^{-1}$ and 1450 - 1600 cm$^{-1}$ are associated with the C-H vibration and the C=C vibration of the benzene ring, respectively. The C-N bonds in the heterocycles are observed at 1320 cm$^{-1}$ [30], and no obvious peaks have been detected above 3000 cm$^{-1}$, suggesting the absence of the amine groups and thus the desired formation of the heterocycles during polymerization, which proves the successful synthesis of TB polymer. With the addition of leaf ZIFs, these peaks become weaker, while those from ZIFs are more significant: C-N of Hmim ligand (995 cm$^{-1}$). Another representative peak (C=N bond, 1305 cm$^{-1}$) is overlapped with the peak of TB, hence it is difficult to be identified. These results represent the blend of the leaf ZIFs into TB polymer matrix.
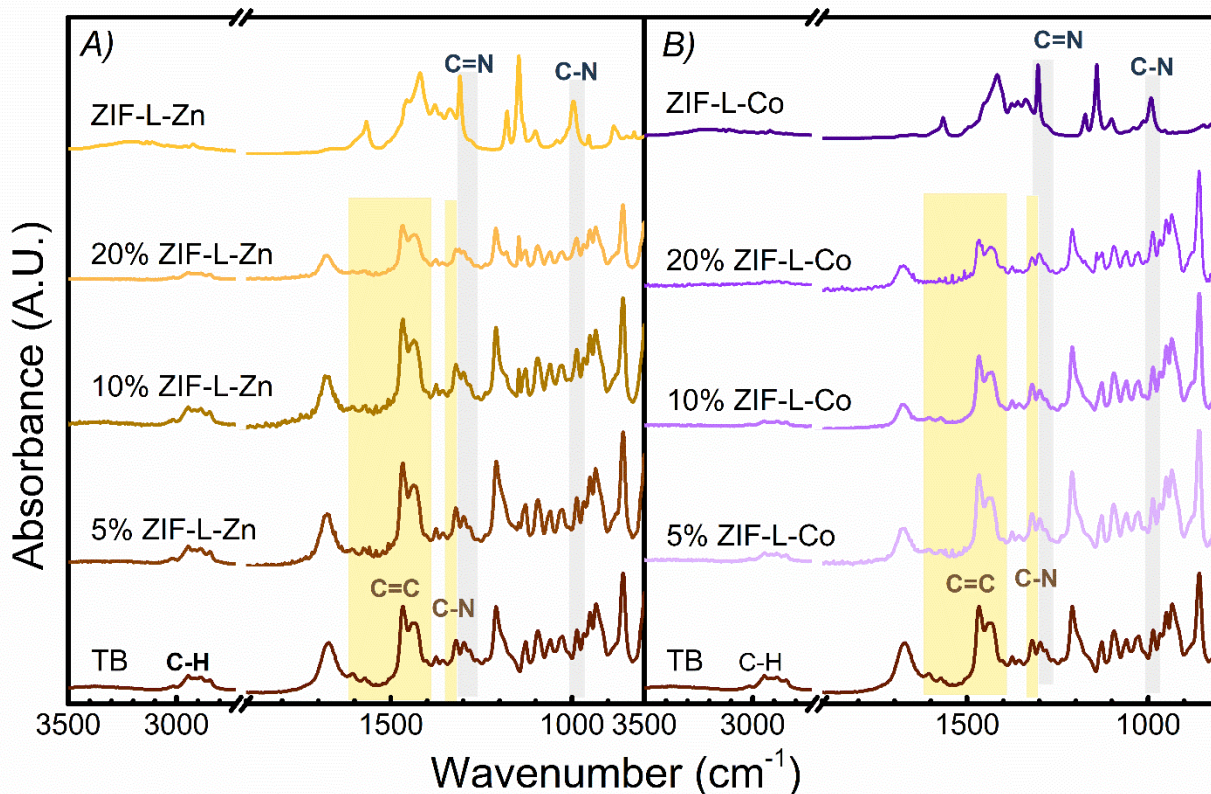
**Figure 2** FTIR spectra of MMMs with different loading of A) ZIF-L-Zn and B) ZIF-L-Co.

## *XRD*

In addition to the FTIR spectra, XRD results can provide valuable information for the MMMs containing crystalline particles. Generally, in XRD results, the sharp and narrow peaks imply higher crystallinity, while the broad and wide ones are usually associated with amorphous materials. In **Figure 3**, the neat TB polymer has two broad peaks at $5^o - 30^o$ and around $41^o$, which are the typical results for amorphous polymers. After the leaf ZIFs were introduced, some sharp and narrow peaks appear, and the intensities of these peaks continue to increase with further addition of ZIFs. Moreover, in the curves of the MMMs with low ZIFs loading, only a few peaks related to the ZIFs are clear, like those at $7.3^o$ and $29.5^o$, while with further increase in ZIF content, more peaks from the ZIFs can be observed, such as peaks at $10.4^o$, $12.8^o$ and $18.0^o$. All these peaks can be found in the pattern of the neat leaf ZIFs. The ones at $7.3^o$ and $18.0^o$ are assigned with the (200) and (004) planes of leaf ZIFs [31]. These findings match the results of the FTIR analysis, implying that these leaf ZIFs have been blended into the polymeric matrix.

10
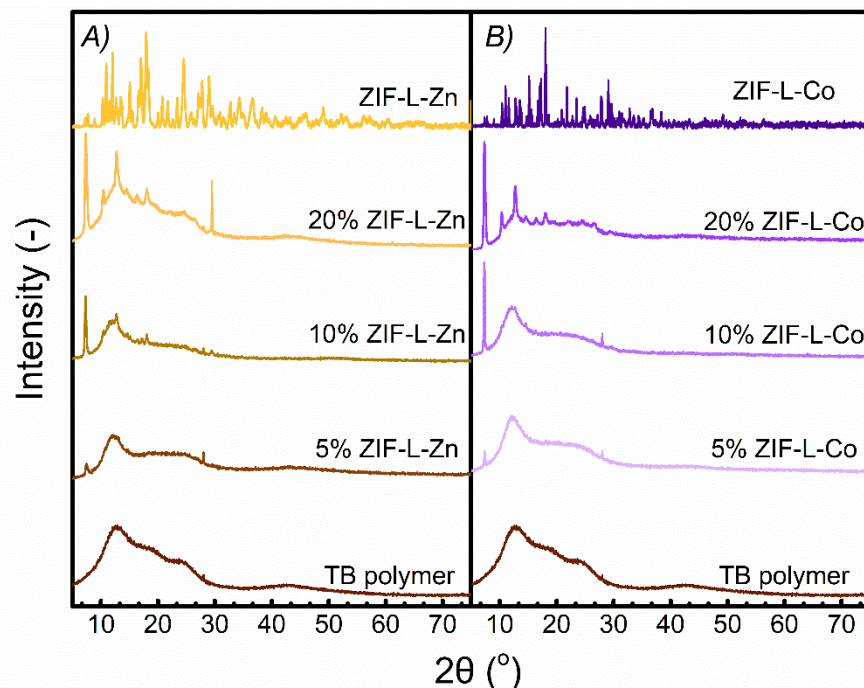
**Figure 3** XRD results of MMMs with different loading of A) ZIF-L-Zn and B) ZIF-L-Co

### *SEM*

In addition to the presence of the ZIFs, the dispersion of the ZIFs in the MMMs plays a great role on the final performance, which can be observed using the SEM. The surface and cross-section images of the MMMs with leaf ZIFs are displayed in **Figure 4**. The neat TB membrane (0% ZIFs) has a uniform and homogenous surface, as well as the cross-section, and no visible defects can be found. After adding leaf ZIFs, the presence of particles changes the morphology of the resultant membranes, making the surface and cross-section more heterogeneous. The leaf ZIFs are wrapped by the polymer chain in the membranes and have been found in the cross-section of the MMMs, even at low ZIF loading (as shown in **Figure 4(B)**). The dispersion of the ZIFs are quite homogenous in the membranes since no apparent aggregation has been found. Moreover, from the SEM images, no clear agglomeration has been detected, suggesting the relatively good compatibility between these leaf ZIFs and TB polymer.
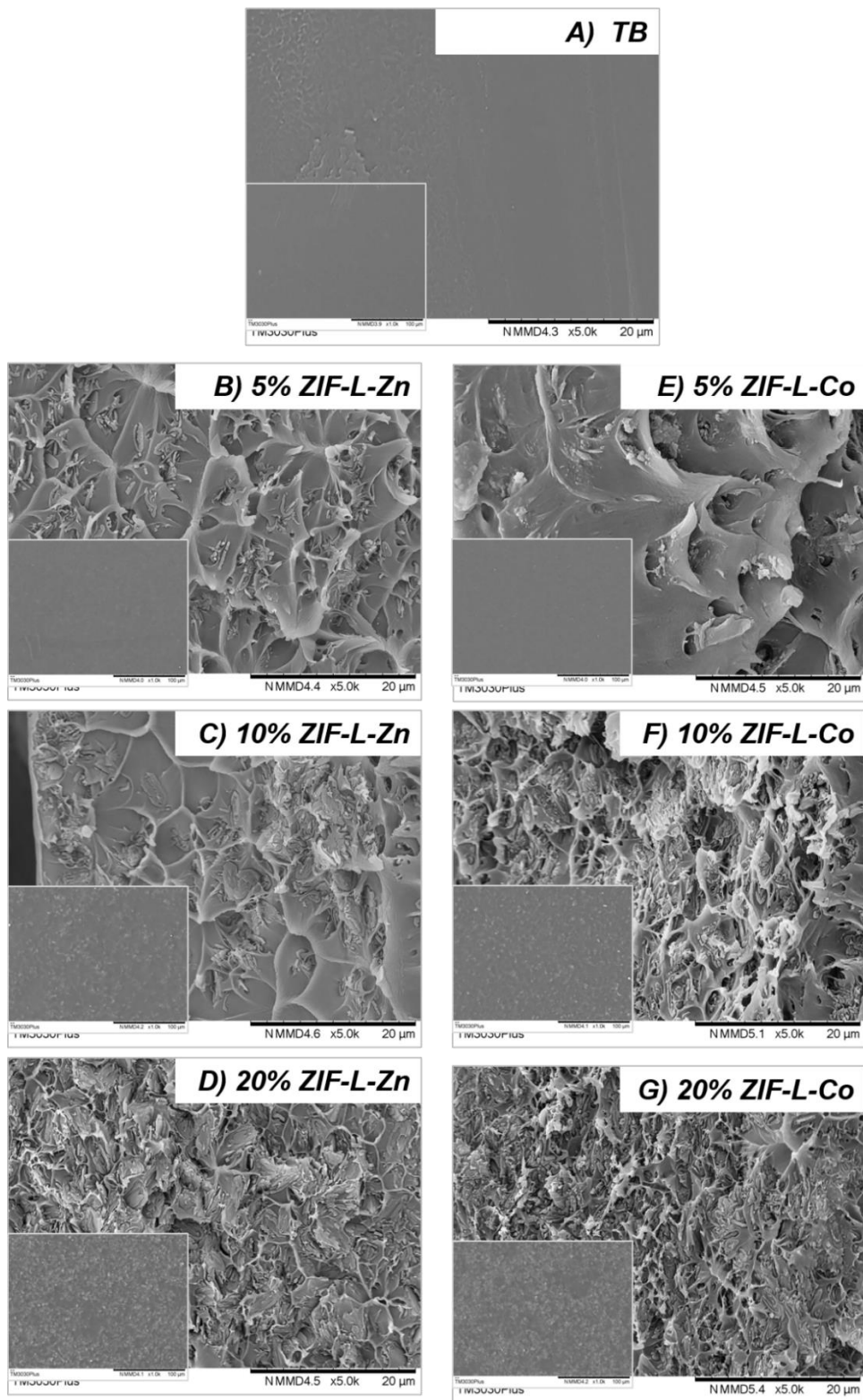
**Figure 4** SEM images of MMMs containing A-D) ZIF-L-Zn and E-G) ZIF-L-Co. The scale bar and magnificantion are 20 µm and 5.0 K for cross-section, and 100 µm and 1.0 K for the insets, respectively.

12

*TGA*

The thermal stability of the membranes with leaf ZIFs was studied by TGA, and the results are displayed in **Figure 5**. For the neat TB polymer, a small amount of weight loss ($< 2\%$) is observed at a low temperature range (R.T. to 100 $^{o}$C), mainly because of the remaining methanol. Afterwards, the mass remains constant until the temperature reaches $\sim$ 400 $^{o}$C, denoting the superior thermal stability of the neat polymer. These MMMs have similar decomposition behavior to the neat polymer: a small weight loss at low temperature due to the remaining methanol, followed by a plateau (100 - 400 $^{o}$C) and then the steep slope starting around 400 $^{o}$C. The $T_{onset}$ decreases with ZIF addition, due to the relative lower decomposition temperature of the ZIFs. However, the changes in $T_{onset}$ are very small, especially for the one with 20 wt.% ZIFs. Considering that the first compound to decompose in ZIFs is the structural water, referring to the weight loss at 150 – 250 $^{o}$C, this enhanced thermal stability may be explained by the removal of structural water inside ZIFs during methanol immersion step, thus leading to an increase in $T_{onset}$.
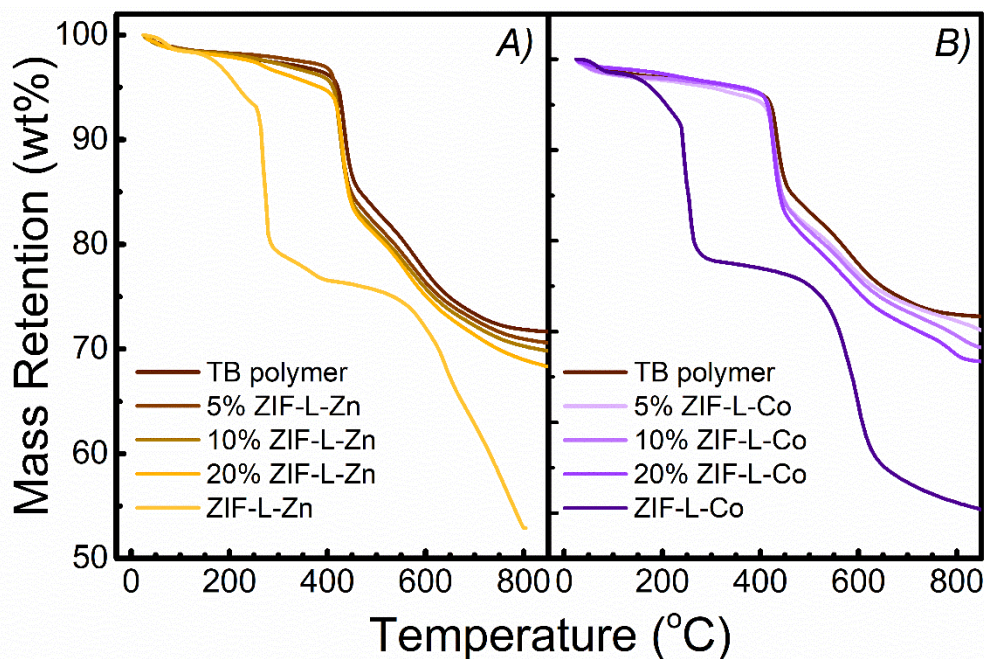


**Figure 5** TGA results of MMMs with different loading of A) ZIF-L-Zn and B) ZIF-L-Co.

## 3.2.2. Gas permeation study

*The effect of leaf ZIF loading*

The gas separation performances of the MMMs containing leaf ZIFs were evaluated by single gas permeation tests at room temperature with a feed pressure of 2 bar. The gas permeabilities of the

membranes with various ZIFs loading are presented in **Figure 6** and **Table S1**. The neat polymeric membrane has a $H_2$ and $CO_2$ permeability of 290.2 and 148.3 Barrer, respectively, in agreement with the values reported in the literature [20]. With the addition of leaf ZIFs, the permeabilities of all investigated gases increase monotonously with ZIF loading. For instance, the addition of ZIF-L-Co (20 wt.%) leads to a 326% and a 272% increase in $H_2$ (1235.5 Barrer) and $CO_2$ permeability (551.6 Barrer), respectively. This significant increment in gas permeability is mainly contributed by the lamellar structure inside these leaf-like ZIFs [23, 25, 32]. Theoretically, the lamellar gaps in 2D ZIFs work as fast shortcuts for those gases small enough to pass through (e.g., $H_2$ and $CO_2$), while for the bulky gases, roundabout pathways must be taken to detour these barriers. As a result, the neat ZIF-L membranes could separate gases more efficiently than by Knudsen diffusion [33], and rationally, the gas permeabilities could gain from these lamellar interlayer channels, which explains the great enhancement in $H_2$ and $CO_2$ permeation. However, for MMMs at high loadings of ZIF-Ls, the experiments showed opposite results from this expectation: The gases with bigger kinetic diameter, like $CH_4$ (3.8 Å) and $N_2$ (3.64 Å) [23], obtained more benefits from the addition of ZIF-L. For example, for membranes with 20 wt.% ZIF-L-Co, 7.5-fold (from 6.2 to 46.5 Barrer) and 8.1-fold (from 6.0 to 49.0 Barrer) increments in $N_2$ and $CH_4$ permeability were observed, respectively. These results imply the existence of more interfacial voids between the fillers and the polymeric matrix at high ZIF-L loadings, which may form nonselective paths, leading to decreasing selectivities, as shown in **Figure 7**. Although the polymer and ZIF-Ls have good compatibility, the interfacial voids are believed not fully avoidable as they are resulted from the less efficient wrap due to the stiff polymer chains or the stress during solvent evaporation [34]. Thus, the $H_2/N_2$ and $H_2/CH_4$ selectivities decrease from 49 to 27 and 50 to 25, respectively, in the presence of 20 wt.% ZIF-L-Co. For $CO_2/N_2$ and $CO_2/CH_4$ selectivities, the values decrease by around 50 %, from 24 to 12 and 25 to 11, respectively. For the $H_2/CO_2$ gas pair, as both gases have similar transport mechanisms, the selectivity remains almost unchanged.
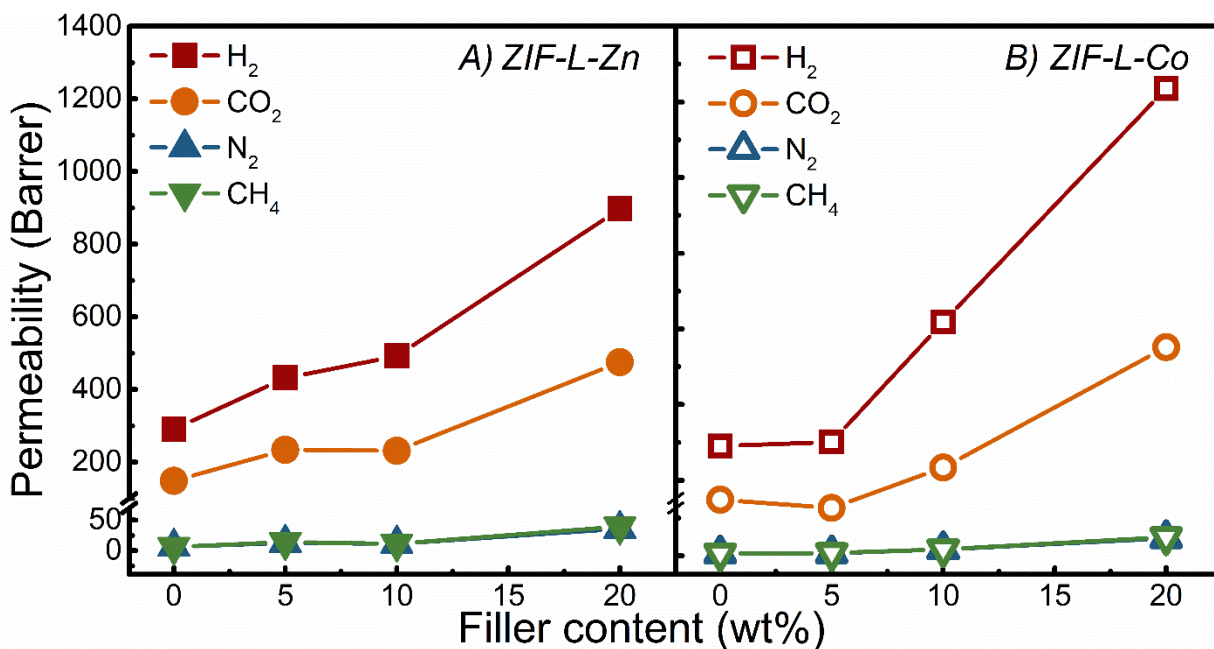
**Figure 6** Gas permeabilities of MMMs with different loading of A) ZIF-L-Zn and B) ZIF-L-Co.

It is well known that, in addition to the filler content, different ZIFs in MMMs will lead to different gas separation performances, mainly due to the differences in crystal structure, chemical nature, interaction with gas species, and their compatibility with the polymeric matrix. In this work, although both leaf ZIFs have identical crystal structure and similar chemical compositions, there still exists some difference between the gas separation performance of MMMs containing ZIF-L-Zn and that of those containing ZIF-L-Co. At low filler loadings, the membranes containing ZIF-L-Zn are more permeable than those with ZIF-L-Co, but by further adding ZIF-L, the gas permeability of TB+ZIF-L-Co membranes increases much fast than their analogies. Hence, at 20 wt.% filler content, the MMMs with ZIF-L-Co display a $H_2$ and $CO_2$ permeabilities of 1235.5 and 551.6 Barrer, respectively, which is 37% and 16% higher than the MMM with Zn-based ZIF. These trends may be explained by several factors. First, despite the same crystal structure and organic linker, the Co-N bonding is stiffer than Zn-N bonds, and thus results in a more rigid framework and smaller aperture (3.3 Å of ZIF-67 compared with 3.4 Å of ZIF-8) [35]. Hence, it is reasonably inferred that the interlayer channels of Co-based ZIF-Ls are smaller than that of the Zn-based ZIF-Ls. This speculation matches with the higher gas permeabilities of MMMs containing 5 wt.% ZIF-L-Zn. However, it is reported that ZIF-67, a Co-based ZIF, has both higher gas sorption rate [36-38] and higher sorption capacities, compared with the Zn-based ZIF-8, which may relate with the interactions between gases and metal sites [39]. The fast sorption rate may counteract the narrower

15

diffusion path in ZIF-L-Co, leading to a more attractive gas diffusion path, especially at higher filler loadings when the fillers brings in more effects. While, the higher gas sorption capacities of Co-based ZIFs [40-43] are beneficial for the gas solubility of the resultant MMMs when the filler loadings increases and the solubility effect becomes more significant. As a result, the membranes with ZIF-L-Co display more significant enhancement on the permeabilities at higher loadings. In terms of the gas selectivities, however, there are far less differences in the effects of the addition of these two ZIFs. The membranes with ZIF-L-Co display slightly higher $H_2$-related selectivity and almost the same $CO_2$-related selectivities compared with the membranes with ZIF-L-Zn. These results suggest that microstructure and the metal ions of these ZIF-Ls have negligible influences on the selectivities in the resultant TB+ZIF-L MMMs.
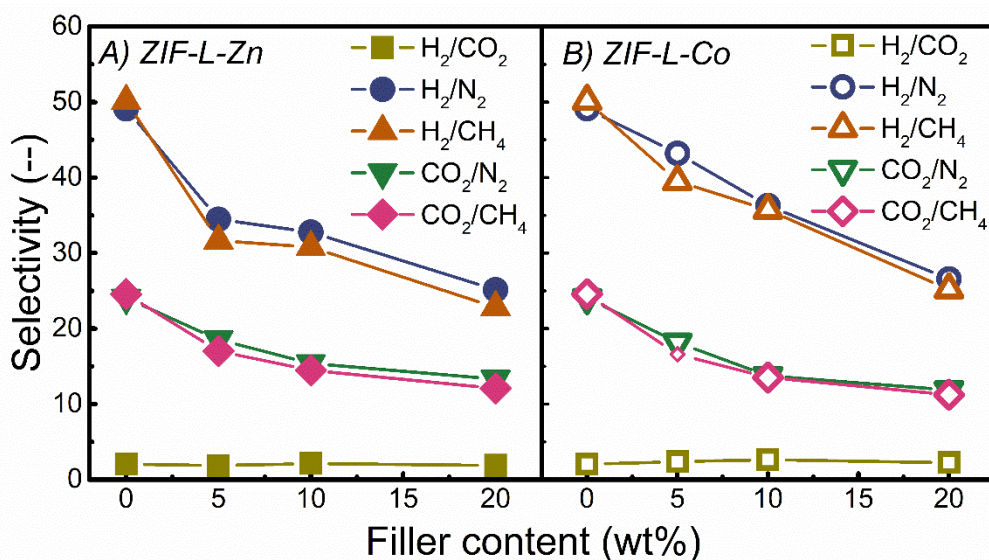


**Figure 7** Gas selectivities of TB + A) ZIF-L-Zn and B) ZIF-L-Co membranes with a function of filler content

To examine these speculations, the diffusivity and solubility of these MMMs were calculated and presented in **Figure 8** and **9**. Because of the extremely fast transport, the time-lag curves of $H_2$ are unnoticeable, and hence the related results are not included here. For the other gases, increased gas diffusivities are observed with the addition of both ZIF-Ls. On the other hand, the addition of ZIF-Ls in general results in decreases in solubility, but to a less significant extent compared with the increases in diffusivity. Hence, the overall effects are shown as increased gas permeability with increasing ZIF-L content.

The different influences of the two ZIF-Ls are also evident in the diffusion and solubility values. At low filler loadings (up to 5 wt. %), the membranes with ZIF-L-Zn have higher gas diffusivities for three gases (i.e., $CO_2$, $N_2$, and $CH_4$), which is believed the result of the bigger interlayer channels. But at higher loadings, the ZIF-L-Co brings about larger increment in the gas diffusivities, which may be related to the higher gas adsorption rate of the Co-based ZIFs compared to the Zn-based ZIFs [36-38]: the faster local absorption-desorption in fillers may promote the faster gas diffusion at high filler loading. In terms of solubility, the membranes containing Co-based ZIF-L display slightly higher solubility, especially in the case of $CO_2$, proving that the ZIF-L-Co is relatively more attractive to the studied gases compared with ZIF-L-Zn [40-43]. Hence, ZIF-L-Co is simultaneously more favorable in both diffusion and solubility than ZIF-L-Zn at higher loadings, leading to higher gas permeabilities. However, considering that the sizes of $N_2$ and $CH_4$ are larger than the channel size of both ZIF-Ls, the increments in the diffusivity of these gases are higher than the one of $CO_2$ with increasing filler loadings and the consequently more interfacial voids, which is believed the main reason for the decreased selectivities. Another reason may be the gate-opening effects [21, 44, 45], which assumes that these ZIFs are flexible and would allow some of the large molecules to pass through, in agreement with the fact that the increment in $CH_4$ diffusivity is less than the gains of $N_2$ diffusivity.
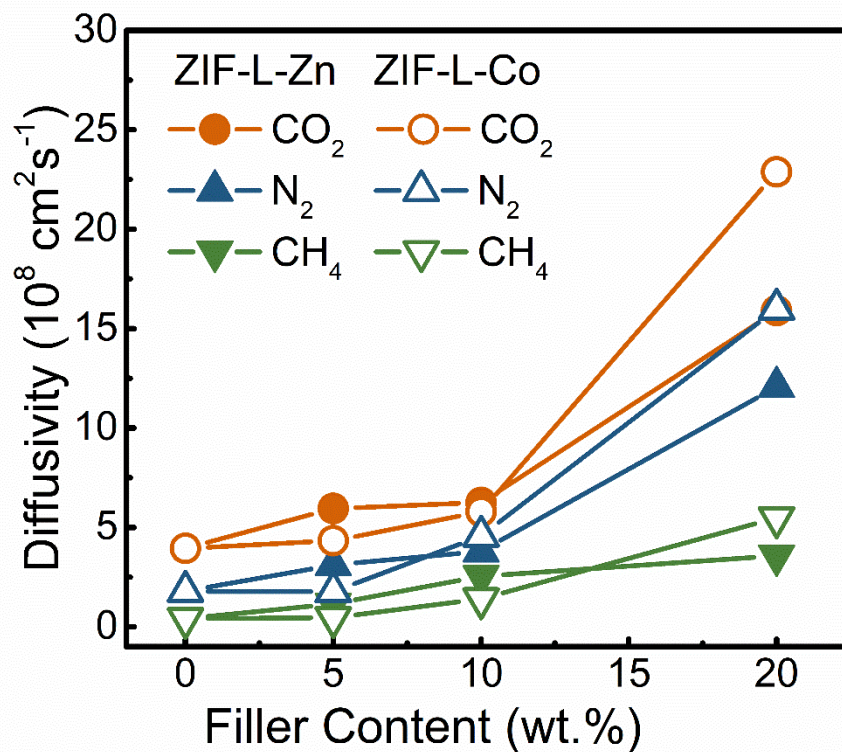
**Figure 8** Gas diffusivity of TB + ZIF-Ls membranes with a function of filler content
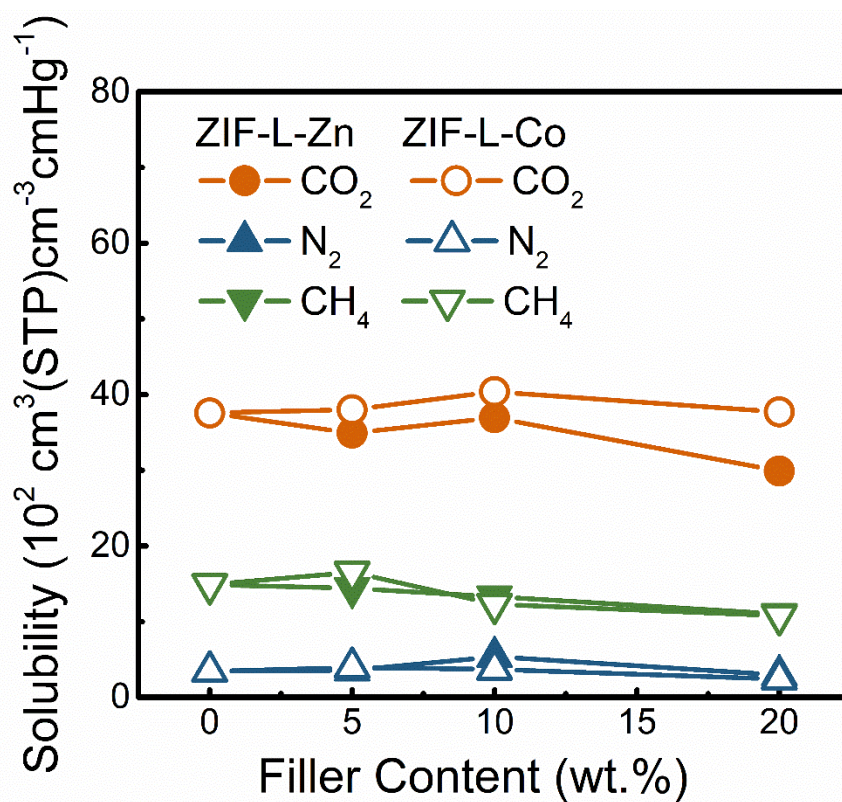


**Figure 9** Gas solubility of TB + ZIF-Ls membranes with a function of filler content

### *The effect of operating temperature*

The ability to efficiently separate gas mixture at relatively high temperature is of great value to some applications, especially for hydrogen separation, which can greatly reduce energy consumption. Moreover, increasing operating temperature usually results in an enhancement in gas diffusivity and thus gas permeability. Due to the high gas permeabilities, the membrane with 20 wt. % ZIF-L-Co was chosen to investigate the effect of temperature, i.e., 24 °C (R.T.), 40 °C and 60 °C.

The permeabilities of all the gases increase greatly with temperature for TB + 20 wt.% ZIF-L-Co membrane, as shown in **Figure 10 (A)**, and this is a typical behavior of diffusion-dominated gas transport in the membrane. At 60 °C, the $H_2$ permeability increases to 1985.9 Barrer, which is 161% of the value obtained at room temperature. It is worth mentioning that the effect of temperature on gas permeability of TB polymer was studied by Fan *et al*., and the results revealed that an increment of ~ 120 % was obtained [20]. Therefore, it is believed that the high value obtained in the present study was mainly because of the fast transport channel brought about by the leaf ZIF-L-Co. All of the gas selectivities in the same work reported by Fan *et al*. decrease with increasing temperature, except for $H_2/CO_2$ selectivity which showed a marginal increase [20]. Neat TB polymer only retains around 65 – 84 % of selectivities of these gas pairs at 65 °C, compared with the values at 35 °C [20]. A similar trend has been observed in our case; selectivities of almost all the gas pairs decreased as temperature increased from RT to 60 °C. The activation energy of gas permeabilities ($E_p$), shown in **Table 1**, was calculated using Arrhenius equation. The $E_p$ is composed of two parts: the activation energy of diffusion ($E_d$) and the heat of sorption ($H_s$), which are usually positive and negative in value, respectively. Hence, the positive $E_p$ means that $E_d$ is higher than $H_s$. Moreover, the activation energy increases with the kinetic diameter of gases, signifying that the larger molecules obtain more benefits from the increased temperature, and that explains the decreased selectivities.
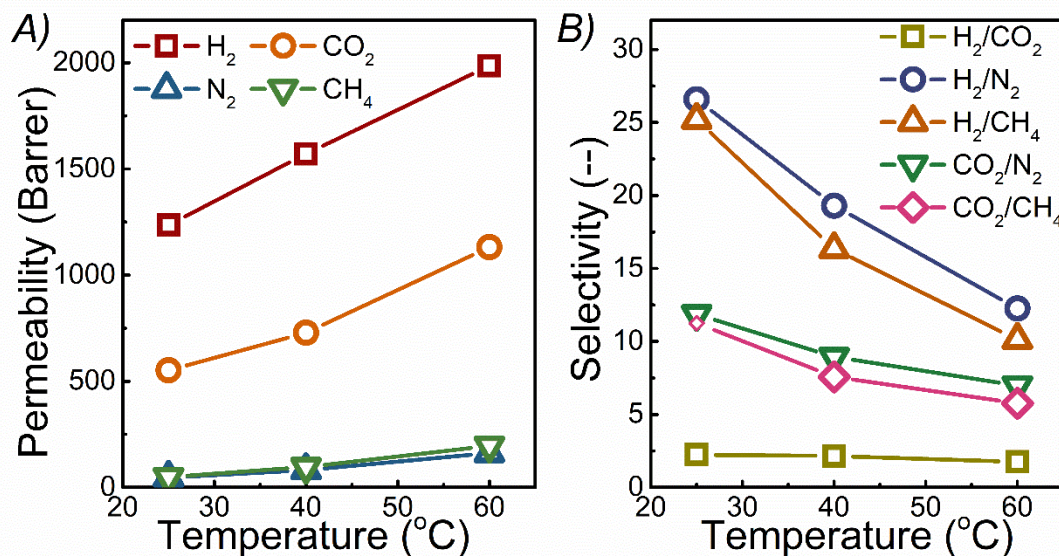
**Figure 10** A) Gas permeabilities and B) selectivities of TB + 20% ZIF-L-Co as a function of operating temperature

**Table 1** Activation energy of permeability of the different gases in TB + 20 % ZIF-L-Co membranes.

| Gas | $H_2$ | $CO_2$ | $N_2$ | $CH_4$ |
|---|---|---|---|---|
| $E_p$ (kJ/mol) | 11.2 | 17.0 | 28.8 | 32.6 |

*Comparison with the Upper Bounds*

The Robeson Upper Bounds have been widely used as benchmarks for the newly developed membrane materials. The gas separation performances of each membrane obtained in this work have been compared with the corresponding Upper Bounds, as shown in **Figure 11**. As discussed previously, the addition of leaf ZIFs results in enhanced gas permeability and reduced selectivities. Therefore, in all figures, the data points move to the bottom right corner with increasing ZIF content or operating temperature. As it can be seen from the figures, for both series of MMMs, applications for $H_2$ separation (e.g., $H_2/CO_2$, $H_2/CH_4$, and $H_2/N_2$) seem more promising than for $CO_2$ separation ($CO_2/N_2$ and $CO_2/CH_4$). It is worth mentioning that the performances of TB + ZIF-L-Co membranes with high filler loadings ($\geq$ 10 wt.%) have passed all Upper Bounds related to $H_2$ separation, thanks to the high $H_2$ permeability. The membranes containing 20 wt.% ZIF-L-Zn have also reached Upper Bounds for all $H_2$ separations.
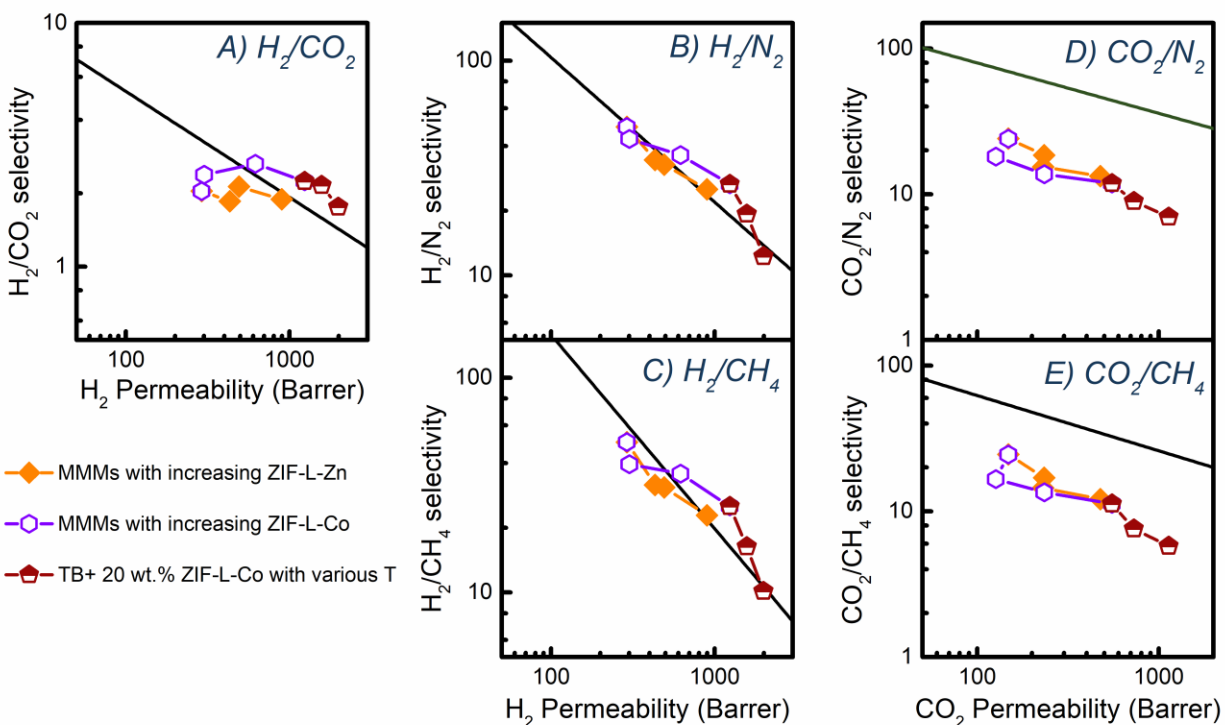
**Figure 11.** Comparison of the pure gas permeation results of the MMMs in this work with the Robeson Upper Bounds (2008).

The performances of some representative state-of-art MMMs are presented in **Table 2** as a comparison of the literature with this work. According to the literature, most of the works on MMMs have been focused on the combination of inorganic fillers with highly permeable polymers, like PIM-1, 6FDA-based polyimide and PTMSP, to ensure the high gas permeation rate. In some studies, inorganic fillers were used mainly to slow down the aging of these high free-volume polymer matrices. In the current work, since TB polymer is much less permeable compared with PIMs and TB-PI (e.g., $H_2$ and $CO_2$ permeabilities of PIM-1 are 3361 Barrer and 5040 Barrer, respectively [22]), the TB+ZIF-L membranes are less permeable than the PIM-1 based and TB-PI based MMMs. Nevertheless, the addition of the ZIF-Ls in this work has brought in a much larger extent of increment in gas permeability compared with, for example, the PIM-1 based MMMs (~1.7-fold increment on both $H_2$ and $CO_2$). On the other hand, some well-known highly $H_2$-selective membrane matrices, like PBI and Matrimid, were also employed to prepare MMMs, but the gas permeability of these MMMs are relatively lower compared with the current work.

**Table 2.** $H_2$ separation or $CO_2$ separation of relevant mixed matrix membranes reported in literature

| Membranes | Permeability (Barrer) | | Selectivity (--) | | | | | Reference |
|---|---|---|---|---|---|---|---|---|
| | $H_2$ | $CO_2$ | $H_2/CO_2$ | $H_2/N_2$ | $H_2/CH_4$ | $CO_2/N_2$ | $CO_2/CH_4$ | |
| PIM-1 + 30 wt.% ZIF-8 [a] | 5456 | 6424 | 0.8 | 17.9 | 14.8 | 21.1 | 17.4 | [22] |
| TOX-PIM-1 + 20 wt.% ZIF-8 [a] | 3465 | 3944 | 0.9 | 24.9 | 23.6 | 28.3 | 26.8 | |
| PIM-1 + 40 wt.% $SiO_2$ [a] | 5544 | 8505 | 0.6 | 9.5 | 6.7 | 14.6 | 10.2 | |
| TOX- PIM-1 + 20 wt.% $SiO_2$ [a] | 2816 | 2615 | 1.1 | 28 | 35 | 26.0 | 32.5 | |
| Matrimid + 15 wt.% ZIF-11 [b] | 535 | - | 9.1 | - | - | - | - | [46] |
| 6FDA-DAM + 20 wt.% ZIF-11 [c] | 272.4 | - | 1.1 | - | 32.8 | - | - | [47] |
| 6FDA-DAM + 8 wt.% Mg-MSS [d] | 794 | 1214 ($CO_2/N_2$); 1245 ($CO_2/CH_4$) | - | - | 21.8 | 24.4 | 31.5 | [48] |
| 6FDA-Durene + 10 wt.% ZIF-71 [e] | 540 | - | 62.5 | - | - | - | - | [21] |
| 6FDA-DAM/HAB + 20 wt% ZIF-L [f] | 260 | 19.4 | 13.4 | 41.4 | 61.6 | 3.1 | 4.6 | [23] |
| TB-PI + 30 wt.% ZIF-8 [g] | 2585 | 1437 | 1.8 | 22 | 28 | 12 | 16 | [24] |
| TB-PI + 30 wt.% PD@ZIF-8 [g] | 1858 | 1056 | 4.3 | 27 | 36 | 14 | 20 | |
| PBI + 58 wt.% Pd [h] | 66 | - | 33 | - | - | - | - | [49] |
| TB + 20 wt% ZIF-L-Zn [j] | 897.5 | 475.4 | 1.9 | 25 | 23 | 13 | 12 | This work |
| TB + 20 wt% ZIF-L-Co [j] | 1235.5 | 551.6 | 2.2 | 27 | 25 | 12 | 11 | |
| TB + 20 wt% ZIF-L-Co [j] | 1985.9 | 1131.5 | 1.8 | 12 | 10 | 7 | 6 | |

[a]: single gas permeation test, feed pressure: 4 bar, 22 °C

[b]: mixed gas permeation test, feed: $H_2/CO_2$ (25/75 vol), 3.3 bar; sweep: Ar, 1.24 bar; 200 °C

[c]: single gas permeation test, feed pressure: 4 bar, 30 °C

[d]: Mg-MSS: Grignard surface functionalized mesoporous silica MCM‐41 spheres; mixed gas permeation test, feed: 50/50 vol for all gas pair, 3.0 bar; sweep: Ar or He, 1.0 bar; 35 °C

[e]: mixed gas permeation test, feed: $H_2/CO_2$ (50/50 vol), 7 atm; vacuum; 35°C- 150°C.

[f]: single gas permeation test, feed pressure: 1 bar, room temperature

[g]: single gas permeation test, feed pressure: 1 bar, 35 °C

[h]: mixed gas permeation test, feed: $H_2/CO_2$ (50/50), 10 bar; sweep: $N_2$, 1 bar; 200 °C

[j]: single gas permeation test, feed pressure: 2 bar, room temperature

# 4 Conclusions

In this work, a series of heterocyclic TB-based polymeric membranes, with two 2D leaf ZIFs (ZIF-L-Zn and ZIF-L-Co) incorporated, have been fabricated and systematically studied using various characterization methods. The relevant characterization results show that both leaf ZIFs have good compatibility with the TB membranes. In addition, all resultant MMMs have excellent thermal stability.

The incorporation of 2D leaf ZIFs results in great enhancement in gas permeabilities for all investigated gases. The addition of 20 wt.% ZIF-L-Co brings about a highly permeable membrane with $H_2$ and $CO_2$ permeability of 1235.5 Barrer and 551.6 Barrer, respectively, which are 4.3 times and 3.7 times of the corresponding gas permeabilities in the neat polymeric membranes. It has also been noticed that the metal centers of the ZIFs could affect their microstructure and therefore the gas transport properties of the resultant MMMs. The Co-based ZIF results in larger increments in gas permeabilites without sacrificing the selectivities, especially for $H_2$, the smallest gas studied in this work, compared with the Zn-based ZIF. Due to the largely increased $H_2$ permeability, all MMMs fabricated using both ZIFs exhibited $H_2$ separation performances close to or surpassing the 2008 Robeson Upper Bounds.

The effects of operating temperature (R.T. to 60 $^o$C) on the gas transport properties of the MMMs with 20% ZIF-L-Co were also evaluated. The increasing temperature could further raise the gas permeabilites: at 60 $^o$C, the $H_2$ permeability reaches 1985.9 Barrer, which is 684% of the values of the neat polymer. In view of the economic consideration and previous process simulation analysis, these highly permeable membranes with moderate selectivity may be an excellent candidate for some industrial applications.

Overall, this work reveals that the metal centers of the ZIFs affect not only the material properties, but also the gas separation performances of the resulting MMMs. Hence, more in-depth studies related to the effects of the chemical structures, especially the metal ions, of the ZIFs on the gas separation performance of the corresponding MMMs are worth undertaking, from which the ZIFs with better gas separation performances could be developed.

## Conflicts of interest

There are no conflicts to declare.

## Acknowledgements

## Supporting Information

The FTIR and TGA results of ZIF-Ls, data of gas permeability, selectivity, diffusivity and solubility of the MMMs, and the changes in gas permeability are supplied as supporting information.

## References

[1] J.A. Turner, Sustainable Hydrogen Production, Science, 305 (2004) 972.

[2] H. Lin, Z. He, Z. Sun, J. Vu, A. Ng, M. Mohammed, J. Kniep, T.C. Merkel, T. Wu, R.C. Lambrecht, $CO_2$-selective membranes for hydrogen production and $CO_2$ capture – Part I: Membrane development, J. Membr. Sci., 457 (2014) 149-161.

[3] P. Li, Z. Wang, Z. Qiao, Y. Liu, X. Cao, W. Li, J. Wang, S. Wang, Recent developments in membranes for efficient hydrogen purification, J. Membr. Sci., 495 (2015) 130-168.

[4] Hydrogen Generation Market Size, Share & Trends Analysis Report By Application (Coal Gasification, Steam Methane Reforming), By Technology, By System (Merchant, Captive), And Segment Forecasts, 2018 - 2025, in, Grand View Research, Inc., 2018.

[5] L. Barelli, G. Bidini, F. Gallorini, S. Servili, Hydrogen production through sorption-enhanced steam methane reforming and membrane technology: A review, Energy, 33 (2008) 554-570.

[6] R. Chaubey, S. Sahu, O.O. James, S. Maity, A review on development of industrial processes and emerging techniques for production of hydrogen from renewable and sustainable sources, Renewable & Sustainable Energy Reviews, 23 (2013) 443-462.

[7] J.D. Holladay, J. Hu, D.L. King, Y. Wang, An overview of hydrogen production technologies, Catal. Today, 139 (2009) 244-260.

[8] S. Thomas, I. Pinnau, N. Du, M.D. Guiver, Pure- and mixed-gas permeation properties of a microporous spirobisindane-based ladder polymer (PIM-1), J. Membr. Sci., 333 (2009) 125-131.

[9] L.M. Robeson, The upper bound revisited, J. Membr. Sci., 320 (2008) 390-400.

[10] Y.B. Zhuang, J.G. Seong, Y.M. Lee, Polyimides containing aliphatic/alicyclic segments in the main chains, Prog. Polym. Sci., 92 (2019) 35-88.

[11] P.M. Budd, B.S. Ghanem, S. Makhseed, N.B. McKeown, K.J. Msayib, C.E. Tattershall, Polymers of intrinsic microporosity (PIMs): robust, solution-processable, organic nanoporous materials, Chem. Commun., (2004) 230-231.

[12] Z.X. Low, P.M. Budd, N.B. McKeown, D.A. Patterson, Gas Permeation Properties, Physical Aging, and Its Mitigation in High Free Volume Glassy Polymers, Chem. Rev., 118 (2018) 5871-5911.

[13] M. Carta, R. Malpass-Evans, M. Croad, Y. Rogan, J.C. Jansen, P. Bernardo, F. Bazzarelli, N.B. McKeown, An efficient polymer molecular sieve for membrane gas separations, Science, 339 (2013) 303-307.

[14] Z.G. Wang, X. Liu, D. Wang, J. Jin, Troger's base-based copolymers with intrinsic microporosity for $CO_2$ separation and effect of Troger's base on separation performance, Polym. Chem., 5 (2014) 2793-2800.

[15] Z.G. Wang, D. Wang, F. Zhang, J. Jin, Troger's Base-Based Microporous Polyimide Membranes for High-Performance Gas Separation, Acs Macro Lett., 3 (2014) 597-601.

[16] J.G. Seong, Y.B. Zhuang, S. Kim, Y.S. Do, W.H. Lee, M.D. Guiver, Y.M. Lee, Effect of methanol treatment on gas sorption and transport behavior of intrinsically microporous polyimide membranes incorporating Troger's base, J. Membr. Sci., 480 (2015) 104-114.

[17] Y. Zhuang, J.G. Seong, Y.S. Do, W.H. Lee, M.J. Lee, M.D. Guiver, Y.M. Lee, High-strength, soluble polyimide membranes incorporating Troger's Base for gas separation, J. Membr. Sci., 504 (2016) 55-65.

[18] Y. Zhuang, J.G. Seong, Y.S. Do, W.H. Lee, M.J. Lee, Z. Cui, A.E. Lozano, M.D. Guiver, Y.M. Lee, Soluble, microporous, Troger's Base copolyimides with tunable membrane performance for gas separation, Chem. Commun., 52 (2016) 3817-3820.

[19] S.S. Zhao, J.Y. Liao, D.F. Li, X.D. Wang, N.W. Li, Blending of compatible polymer of intrinsic microporosity (PIM-1) with Troger's Base polymer for gas separation membranes, J. Membr. Sci., 566 (2018) 77-86.

[20] Y.F. Fan, C. Li, X.S. Zhang, X.M. Yang, X.Y. Su, H.M. Ye, N.W. Li, Troger's base mixed matrix membranes for gas separation incorporating $NH_2$-MIL-53(Al) nanocrystals, J. Membr. Sci., 573 (2019) 359-369.

[21] S. Japip, K.-S. Liao, T.-S. Chung, Molecularly Tuned Free Volume of Vapor Cross-Linked 6FDA-Durene/ZIF-71 MMMs for $H_2$/$CO_2$ Separation at 150 °C, Adv. Mater., 29 (2017) 1603833.

[22] Q. Song, S. Cao, R.H. Pritchard, H. Qiblawey, E.M. Terentjev, A.K. Cheetham, E. Sivaniah, Nanofiller-tuned microporous polymer molecular sieves for energy and environmental processes, J. Mater. Chem. A, 4 (2016) 270-279.

[23] S. Kim, E. Shamsaei, X. Lin, Y. Hu, G.P. Simon, J.G. Seong, J.S. Kim, W.H. Lee, Y.M. Lee, H. Wang, The enhanced hydrogen separation performance of mixed matrix membranes by incorporation of two-dimensional ZIF-L into polyimide containing hydroxyl group, J. Membr. Sci., 549 (2018) 260-266.

[24] Z. Wang, D. Wang, S. Zhang, L. Hu, J. Jin, Interfacial Design of Mixed Matrix Membranes for Improved Gas Separation Performance, Adv. Mater., 28 (2016) 3399-3405.

[25] R. Chen, J. Yao, Q. Gu, S. Smeets, C. Baerlocher, H. Gu, D. Zhu, W. Morris, O.M. Yaghi, H. Wang, A two-dimensional zeolitic imidazolate framework with a cushion-shaped cavity for $CO_2$ adsorption, Chem. Commun., 49 (2013) 9500-9502.

[26] Y. Lo, C.H. Lam, C.-W. Chang, A.-C. Yang, D.-Y. Kang, Polymorphism/pseudopolymorphism of metal–organic frameworks composed of zinc (II) and 2-methylimidazole: synthesis, stability, and application in gas storage, RSC Adv., 6 (2016) 89148-89156.

[27] A.M. Nasir, N.A.H. Md Nordin, P.S. Goh, A.F. Ismail, Application of two-dimensional leaf-shaped zeolitic imidazolate framework (2D ZIF-L) as arsenite adsorbent: Kinetic, isotherm and mechanism, J. Mol. Liq., 250 (2018) 269-277.

[28] X. Li, Z. Li, L. Lu, L. Huang, L. Xiang, J. Shen, S. Liu, D.R. Xiao, The Solvent Induced Inter-Dimensional Phase Transformations of Cobalt Zeolitic-Imidazolate Frameworks, Chem. Eur. J., 23 (2017) 10638-10643.

[29] Z.-X. Low, J. Yao, Q. Liu, M. He, Z. Wang, A.K. Suresh, J. Bellare, H. Wang, Crystal transformation in zeolitic-imidazolate framework, Cryst. Growth Des., 14 (2014) 6589-6598.

[30] Y. Cui, Y. Liu, J. Liu, J. Du, Y. Yu, S. Wang, Z. Liang, J. Yu, Multifunctional porous Tröger's base polymers with tetraphenylethene units: $CO_2$ adsorption, luminescence and sensing properties, Polym. Chem., 8 (2017) 4842-4848.

[31] H. Mao, H.-G. Zhen, A. Ahmad, S.-H. Li, Y. Liang, J.-F. Ding, Y. Wu, L.-Z. Li, Z.-P. Zhao, Highly selective and robust PDMS mixed matrix membranes by embedding two-dimensional ZIF-L for alcohol permselective pervaporation, J. Membr. Sci., 582 (2019) 307-321.

[32] J. Shen, G. Liu, K. Huang, W. Jin, K.-R. Lee, N. Xu, Membranes with Fast and Selective Gas-Transport Channels of Laminar Graphene Oxide for Efficient $CO_2$ Capture, Angew. Chem., 127 (2015) 588-592.

[33] Z. Zhong, J. Yao, R. Chen, Z. Low, M. He, J.Z. Liu, H. Wang, Oriented two-dimensional zeolitic imidazolate framework-L membranes and their gas permeation properties, J. Mater. Chem. A, 3 (2015) 15715-15722.

[34] R. Mahajan, R. Burns, M. Schaeffer, W.J. Koros, Challenges in forming successful mixed matrix membranes with rigid polymeric materials, J. Appl. Polym. Sci., 86 (2002) 881-890.

[35] P. Krokidas, M. Castier, I.G. Economou, Computational study of ZIF-8 and ZIF-67 performance for separation of gas mixtures, The Journal of Physical Chemistry C, 121 (2017) 17999-18011.

[36] C. Wang, F. Yang, L. Sheng, J. Yu, K. Yao, L. Zhang, Y. Pan, Zinc-substituted ZIF-67 nanocrystals and polycrystalline membranes for propylene/propane separation, Chem. Commun., 52 (2016) 12578-12581.

[37] P. Krokidas, M. Castier, S. Moncho, D.N. Sredojevic, E.N. Brothers, H.T. Kwon, H.-K. Jeong, J.S. Lee, I.G. Economou, ZIF-67 Framework: A Promising New Candidate for Propylene/Propane Separation. Experimental Data and Molecular Simulations, The Journal of Physical Chemistry C, 120 (2016) 8116-8124.

[38] A. Awadallah-F, F. Hillman, S.A. Al-Muhtaseb, H.-K. Jeong, Nano-gate opening pressures for the adsorption of isobutane, n-butane, propane, and propylene gases on bimetallic Co–Zn based zeolitic imidazolate frameworks, Dalton Transactions, 48 (2019) 4685-4695.

[39] E. Atci, S. Keskin, Understanding the Potential of Zeolite Imidazolate Framework Membranes in Gas Separations Using Atomically Detailed Calculations, The Journal of Physical Chemistry C, 116 (2012) 15525-15537.

[40] A. Zanon, S. Chaemchuen, B. Mousavi, F. Verpoort, 1 Zn-doped ZIF-67 as catalyst for the $CO_2$ fixation into cyclic carbonates, Journal of $CO_2$ Utilization, 20 (2017) 282-291.

[41] D.K. Panchariya, R.K. Rai, E. Anil Kumar, S.K. Singh, Core–Shell Zeolitic Imidazolate Frameworks for Enhanced Hydrogen Storage, ACS Omega, 3 (2018) 167-175.

[42] K. Zhou, B. Mousavi, Z. Luo, S. Phatanasri, S. Chaemchuen, F. Verpoort, Characterization and properties of Zn/Co zeolitic imidazolate frameworks vs. ZIF-8 and ZIF-67, J. Mater. Chem. A, 5 (2017) 952-957.

[43] G. Kaur, R.K. Rai, D. Tyagi, X. Yao, P.-Z. Li, X.-C. Yang, Y. Zhao, Q. Xu, S.K. Singh, Room-temperature synthesis of bimetallic Co–Zn based zeolitic imidazolate frameworks in water for enhanced $CO_2$ and $H_2$ uptakes, J. Mater. Chem. A, 4 (2016) 14932-14938.

[44] D. Fairen-Jimenez, S.A. Moggach, M.T. Wharmby, P.A. Wright, S. Parsons, T. Düren, Opening the Gate: Framework Flexibility in ZIF-8 Explored by Experiments and Simulations, J. Am. Chem. Soc., 133 (2011) 8900-8902.

[45] L. Zhang, Z. Hu, J. Jiang, Sorption-Induced Structural Transition of Zeolitic Imidazolate Framework-8: A Hybrid Molecular Simulation Study, J. Am. Chem. Soc., 135 (2013) 3722-3728.

[46] J. Sánchez-Laínez, B. Zornoza, Á. Mayoral, Á. Berenguer-Murcia, D. Cazorla-Amorós, C. Téllez, J. Coronas, Beyond the $H_2/CO_2$ upper bound: one-step crystallization and separation of nano-sized ZIF-11 by centrifugation and its application in mixed matrix membranes, J. Mater. Chem. A, 3 (2015) 6549-6556.

[47] M. Safak Boroglu, A.B. Yumru, Gas separation performance of 6FDA-DAM-ZIF-11 mixed-matrix membranes for $H_2/CH_4$ and $CO_2/CH_4$ separation, Sep. Purif. Technol., 173 (2017) 269-279.

[48] B. Zornoza, C. Téllez, J. Coronas, O. Esekhile, W.J. Koros, Mixed matrix membranes based on 6FDA polyimide with silica and zeolite microsphere dispersed phases, AlChE J., 61 (2015) 4481-4490.

[49] L. Zhu, D. Yin, Y. Qin, S. Konda, S. Zhang, A. Zhu, S. Liu, T. Xu, M.T. Swihart, H. Lin, Sorption-Enhanced Mixed Matrix Membranes with Facilitated Hydrogen Transport for Hydrogen Purification and $CO_2$ Capture, Adv. Funct. Mater., 29 (2019) 1904357.